

Review

Characterization of Pb-Free KNbO_3 - and $(\text{Na,Bi})\text{TiO}_3$ -Based Piezoelectric Single-Crystals Using X-ray and Neutron Diffraction

Abhijit Pramanick

Department of Materials Science and Engineering, City University of Hong Kong, Hong Kong SAR, China; apramani@cityu.edu.hk; Tel.: +852-5972-2084

Received: 19 December 2017; Accepted: 10 January 2018; Published: 19 January 2018

Abstract: In view of serious environmental concerns with traditional Pb-based piezoelectrics, the search for new Pb-free alternatives has intensified recently. A thorough investigation of structure-property relationships in Pb-free piezoelectrics is desired in order to design new material compositions with high electromechanical properties that can be operated over a broader range of conditions. Recent availability of high-quality single crystals has not only opened the possibility for achieving multifold enhancements in the electromechanical properties in this new class of materials, but has also provided opportunities to undertake fundamental studies on their structure-property relationships. In the following pages, I review some of the recent X-ray and neutron diffraction studies of Pb-free piezoelectric single crystals, which have provided novel insights into their multiscale stimuli-induced structural mechanisms, including phase transitions, nanoscale structural ordering, lattice instability, and domain re-orientation. Opportunities and challenges for future progress in this area of study are discussed.

Keywords: Pb-free piezoelectrics; single-crystals; X-ray and neutron diffraction

1. Introduction

Piezoelectricity is the coupling between dielectric and elastic displacements in a material that are induced under the effects of an applied mechanical stress or electric field [1]. The piezoelectric effect is necessarily observed in materials with non-centrosymmetric crystal structures. Large piezoelectric effects are observed in ferroelectric materials, for which each crystallographic unit cell also exhibits a spontaneous and reversible polarization or dipole moment under practical conditions [2]. Owing to the large electro-mechanical coupling phenomena in ferroelectric materials, they are of interest for a broad array of applications including precision actuators, impact and load sensors, telecommunication, and biomedical imaging [3–5]. With growing innovation in sectors such as internet of things (IoT), mechatronics, and decentralized energy harvesting, a large jump in the usage of ferroelectric materials as smart electromechanical transducers can be foreseen in the future.

Traditionally, the industry for ferroelectrics in electromechanical applications has been dominated by materials with high Pb-content [6]. For example, the most popular industrial piezoelectrics, such as $\text{Pb}(\text{Zr}_x\text{Ti}_{1-x})\text{O}_3$ (PZT) and $\text{PbMg}_{1/3}\text{Nb}_{2/3}\text{O}_3$ - PbTiO_3 (PMN-PT), contain up to 60% Pb by weight. Pb is known to be toxic to the functioning of biological life-forms. Although Pb is usually stable in oxide form, it can eventually leak into the environment upon disposal over the long-term, and therefore poses danger to the ecosystem. Consequently, a larger scale adoption of Pb-based ferroelectrics is foreseen to pose serious environmental danger. With such foresight, more stringent regulations on the use of Pb in electronic materials are being imposed by several agencies worldwide [7–10]. In view of this, the development of Pb-free ferroelectrics with electromechanical properties at par with or exceeding those of Pb-based ferroelectrics is of utmost importance [11].

Indeed, intensive research efforts over the last decade have led to the development of several Pb-free alternatives for ferroelectric piezoelectrics. The Pb-free piezoceramics that have gained much attention include those based on certain prototypical formulations, such as potassium sodium niobate or (K,Na)NbO₃ (KNN), sodium bismuth titanate or (Na,Bi)TiO₃ (NBT), and solid solutions of barium titanate such as Ba(Zr,Ti)O₃ and (Ba,Ca)(Zr,Ti)O₃ (BZT and BCZT). Research into each of these material categories was triggered by some of the pioneering works such as [12–14]. An important property index of interest, with regard to sensor applications, is the direct piezoelectric coefficient d_{33} , which is the ratio between the amounts of electrical charge generated with respect to the applied mechanical stress amplitude. Similarly, an important property index of piezoelectric materials for application in actuators is the converse piezoelectric strain coefficient d_{33}^* , which is the amount of strain produced with respect to the amplitude of the applied electric field or E . Figure 1a compares d_{33}^* and usable temperature range of the industry standard of Pb-based PZT and the different classes of Pb-free piezoceramics [11]. The maximum usable temperature range is defined by either the ferroelectric-to-paraelectric phase transition temperature T_C or the depoling temperature T_d , beyond which a drastic reduction in d_{33} or d_{33}^* can be observed. As shown in Figure 1a, while the properties of many of the Pb-free piezoceramics are quite impressive in individual respects, none of the Pb-free piezoceramics compare favorably with PZT in terms of both d_{33}^* and usable temperature range. Therefore, further optimization of the properties of Pb-free piezoelectric materials is desirable. Such developments need to be in conjunction with improvements in other aspects, such as energy efficiency and ease of synthesis, for their eventual widespread adoption.

Synthesis of ferroelectric materials in their single-crystal form provides one possible means for achieving multifold enhancement in electromechanical properties. This is due to the anisotropic nature of piezoelectric properties in ferroelectric crystals, which can be anomalously higher for certain crystallographic directions. For example, while the longitudinal piezoelectric coefficient d_{33} for polycrystalline PMN-PT is ~200 pC/N, the same for single crystal PMN-PT is ~2800 pC/N when poled along [001] but ~190 pC/N when poled along [111] [5]. Similar anisotropic enhancements in shear piezoelectric coefficients can also be observed, such as that a value of d_{15} ~2500 pC/N is observed in PMN-PT single-crystal when poled along [011] [5]. In addition to the intrinsic piezoelectric anisotropy of ferroelectric crystals, enhancement in electromechanical property coefficients can also be induced from certain configurations of ferroelectric domains, otherwise known as domain-engineering; however, there exists debate about the underlying mechanisms for the same, such as [15–19].

Enhancements in piezoelectric properties of Pb-free ferroelectric single-crystals can be similarly predicted based on both theoretical and experimental studies. For example, Davis et al. showed from phenomenological calculations that the longitudinal d_{33}^* in prototypical BaTiO₃ is expected to be higher for crystallographic directions away from the polar axis of [001] [20]. Experimentally, large anisotropic enhancements in piezoelectric coefficients were observed for BaTiO₃ single-crystals by Wada et al., such as a maximum d_{31}^* ~230 pC/N when poled along [111] direction and a maximum d_{33}^* ~500 pC/N for [001] oriented orthorhombic BaTiO₃ crystal [21,22]. It is therefore worthy to pursue possible enhancements in the electromechanical properties of Pb-free ferroelectrics by growing single-crystals with preferred orientations. An example of a recent development in this area is shown in Figure 1b, where large anisotropic enhancement in electric-field-induced strain is observed for a single-crystal of Pb-free (K_{0.25}Na_{0.75})NbO₃ [23].

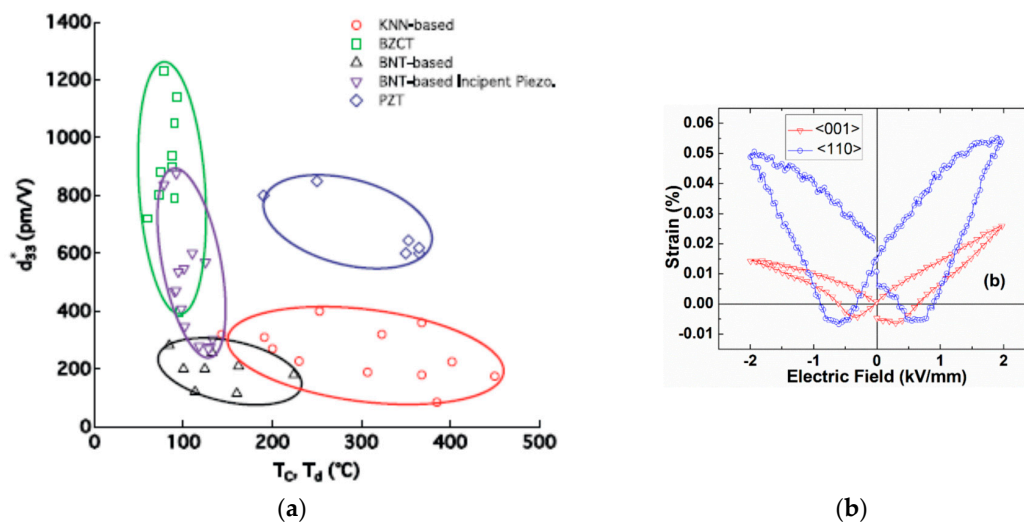


Figure 1. (a) A comparison of converse piezoelectric coefficient and maximum usable temperature for different classes of Pb-free and Pb-based piezoelectric ceramics. Reprinted from J. Eur. Ceram. Soc., 35, Rödel et al., “Transferring lead-free piezoelectric ceramics into applications”, 1659–1681, Copyright (2015), with permission from Elsevier. (b) Orientation dependent enhancement in electric-field-induced strains in (K,Na)NbO₃ (KNN) single crystal [23].

However, a limiting factor for broader investigation of Pb-free ferroelectric single crystals could be difficulties in synthesizing crystals of adequate dimensions and quality. In this respect, recent advancements on synthesis of good quality Pb-free piezoelectric single crystals of complex compositions with high functional properties is an exciting development. Notable mentions in this category include crystals of Li-doped potassium sodium niobate using the Bridgman method [24], $(1-x)\text{BaTiO}_3-x\text{CaTiO}_3$ using floating zone technique [25], $(\text{Ba}_{(1-x)}\text{Ca}_x)(\text{Ti}_{(1-y)}\text{Zr}_y)\text{O}_3$ by Chochralski method [26], $(\text{Ba}_{(1-x)}\text{Ca}_x)(\text{Ti}_{(1-y)}\text{Zr}_y)\text{O}_3$ by the flux-method [27], $(\text{Na}_{0.5}\text{Bi}_{0.5})\text{TiO}_3\text{-BaTiO}_3$ and $(\text{K,Na})(\text{Nb,Ta})\text{O}_3$ using the top-seeded solution growth (TSSG) method [23,28–30], and $(\text{Na}_{0.5}\text{Bi}_{0.5})\text{TiO}_3\text{-BaTiO}_3$ - and $(\text{K,Na})(\text{Nb})\text{O}_3$ -based crystals using the seed-free solid state crystal growth technique [31–33]. The developments with regard to solid state crystal growth are particularly noteworthy, since they provide a cheaper alternative to growing crystals from melt. An exhaustive review on the art of converting polycrystalline ceramics to single-crystalline form for Pb-free ferroelectrics is given by Kang et al. [34].

2. Characterization of Multiscale Structural Mechanisms Using Diffraction

The above mentioned recent developments towards synthesis of Pb-free ferroelectric single crystals are not only exciting from the perspective of achieving higher properties, but they can also facilitate better identification of the fundamental physical mechanisms responsible for electromechanical responses. The macroscopic electromechanical responses in a ferroelectric material, including both stress-induced polarization and electric-field-induced strains, are the result of structural changes that are operative at multiple length scales—these include atomic displacements and distortion of crystallographic unit cell, short-range ordering within nanoscale polar clusters, and motion of ferroelectric/ferroelastic domain boundaries (Figure 2) [5,35,36]. A clear identification of the prevalence of each of these structural mechanisms in materials of different compositions and their respective roles towards enhancement of macroscopic properties can lead to faster development of new Pb-free ferroelectrics. High-energy X-ray and neutron diffraction (or scattering in general) experiments of materials under applied external stimuli has been a preferred method of investigation for identification of microscopic structural mechanisms in a wide variety of materials. Reasons for such a preference include easy sample preparation, the option of gaining structural information from bulk material

volume, ease of designing sample environments, and relatively faster data collection. In situ diffraction experiments have been broadly applied in the past to identify the microscopic structural mechanisms operative under external electric fields or stress in both single-crystal and polycrystalline forms of Pb-based ferroelectrics [37]. In particular, diffraction experiments in single-crystalline materials were instrumental in identifying subtler changes in materials structure, which are not readily observable from experiments with polycrystalline ceramics, such as small distortions from ground-state crystal symmetry, changes in nanoscale ordering, and domain reorientation pathways [38–40].

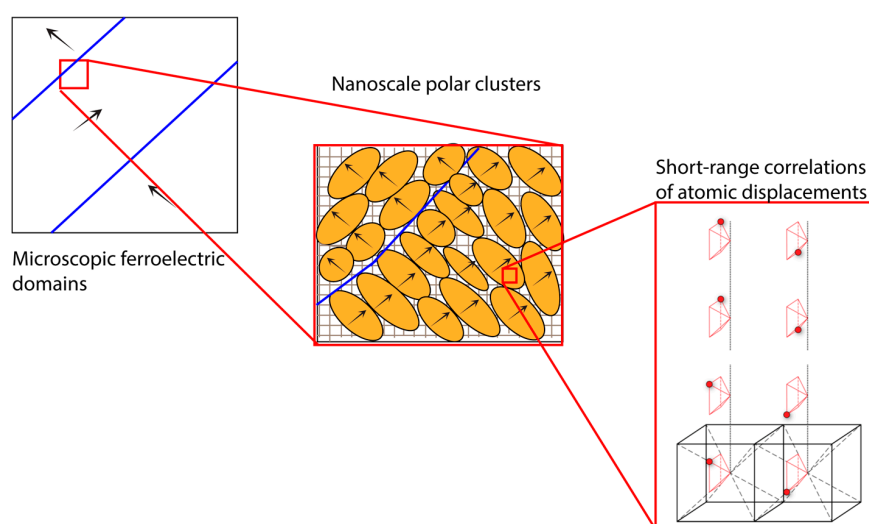


Figure 2. Schematic illustration of multi-level structural hierarchy in single-crystals of Pb-free piezoelectric materials. Application of external stimuli induces changes for one or more of the structural features.

Recent advancements with regard to available flux and resolution for diffraction experiments has broadened the scope and precision of structural insights that can be gained from in situ experiments. Indeed, advanced diffraction experiments on polycrystalline ceramics have elucidated several electric field and/or stress-induced structural mechanisms that are unique to Pb-free piezoelectrics. A review of these developments can be found in references [41,42]. Nevertheless, similar reviews on single-crystal diffraction experiments of Pb-free piezoelectrics are absent. The author is of the opinion that such a review on the study of structure-property correlations of Pb-free piezoelectrics using single-crystal diffraction is warranted in view of recent developments and potential opportunities.

2.1. Crystallographic Phase Transition

External stimuli induced changes in the original crystal structure of a ferroelectric crystal constitutes the intrinsic component of its electromechanical response. Without consideration to local structural disorders, this involves changes in the relative atomic positions within the unit cell that defines the *average long-range* crystallographic structure. It is debatable whether the alteration in atomic arrangements constitutes a structural distortion or true phase transition, which are different for specific cases [20]. Nevertheless, it is important to identify such structural mechanisms to understand material behavior from a fundamental perspective and to explore possible avenues for enhancement in electromechanical properties. Diffraction is widely used as an experimental tool for characterization of stimuli-induced crystallographic phase transitions (or distortions) in ferroelectrics. The crystallographic structural changes can be characterized from data collected in a diffraction experiment by monitoring changes in some essential features, such as *hkl* diffraction peak position to determine changes in lattice planes spacing and splitting of *hkl* reflections to identify changes in crystallographic symmetry. In addition, change in intensities of *hkl* reflections can reflect various crystallographic and microstructural changes such as relative positions of different ions, state of

microstructural defects, as well as internal strains, which can be distinguished based on quantitative modeling [36,37,41–44].

The scattered intensity is essentially a Fourier transformation of the microscopic arrangement of the atoms inside a material. This can be represented as,

$$I(\vec{Q}) = \sum_{n=1}^N \sum_{m=1}^N f_m f_n \exp\left(i\vec{Q} \cdot (\vec{R}_m - \vec{R}_n)\right) \quad (1)$$

where N is the total number of atoms and f_m is the scattering factor of an atom m that is located at the lattice site at the location \vec{R}_m . The scattering factor is different for different elements, depending on the interaction of the X-rays with the electron clouds of the atoms or the interaction of the neutrons with the atomic nuclei. It can be readily seen from Equation (1) that the intensities of the diffracted beams are very sensitive to the arrangement of atoms in a crystal. The diffraction pattern from polycrystalline ceramics constitutes a summation of scattering intensities from different oriented crystallites within the sample, which is presented either as a 1-dimensional line profile with multiple hkl diffraction peaks or concentric circles of hkl reflections, depending on specific experimental geometry. Diffraction from polycrystalline ceramic samples are often adequate to identify and characterize many of changes as listed above. However, in other cases, single-crystal diffraction experiments are necessary for characterization of subtler changes in crystal symmetry, which can otherwise remain elusive. For example, high-resolution single-crystal diffraction has been particularly helpful in clearly identifying monoclinic structural distortions and polarization reorientation mechanism in Pb-based relaxor ferroelectric materials [38]. Although such experiments are not yet commonplace for Pb-free ferroelectric materials, examples from some recent studies are reviewed below.

Kreisel et al. used high-energy X-ray diffraction of $\text{Na}_{0.5}\text{Bi}_{0.5}\text{TiO}_3$ single crystals to show a series of phase transitions induced under the application of mechanical pressure which were identified from splitting of diffraction peaks, such as shown in Figure 3 [45]. A rhombohedral-to-monoclinic transition was observed at lower pressures, while a further transition to tetragonal phase could be observed under a pressure of 11 GPa. Although a similar phase transition was also shown from diffraction measurements of polycrystalline ceramic samples, single-crystal diffraction provided a more definitive description of structural mechanisms involving correlated symmetry changes and octahedral tilting.

In yet another interesting experiment, Ogino et al. determined the polarization rotation pathway for the average monoclinic crystal structure in a $\text{Na}_{0.5}\text{Bi}_{0.5}\text{TiO}_3$ - BaTiO_3 single crystal sample [30]. Based on detailed analysis of diffraction spot positions, and further assisted by DFT calculations, the authors showed that the polarization vector rotates by $\sim 2^\circ$ in the monoclinic a - c plane when an electric field E of 70 kV/cm is applied along $\langle 001 \rangle$ pseudo-cubic direction.

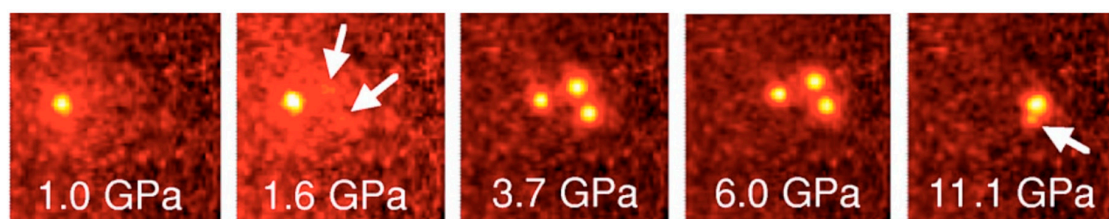


Figure 3. In situ diffraction experiment on a $\text{Na}_{0.5}\text{Bi}_{0.5}\text{TiO}_3$ single-crystal shows changes in 300 reflections as a function of applied pressure. Symmetry-related peak splitting indicates gradual cross-over from rhombohedral-to-monoclinic-to-tetragonal phases with increasing applied pressure. The arrows indicate the appearance of additional peaks. After Kreisel et al. Reprinted from reference [45] DOI: 10.1103/PhysRevB.68.014113, with permission from the American Physical Society.

2.2. Nanoscale Structural Disorders

In many ferroelectrics, the optimum electromechanical properties often correlate with the presence of nanoscale structural disorders. This means that while translational periodicity of the crystal

lattice is maintained *on average*, there are local deviations from the average structure because of energetically degenerate quasi-random structural features such as atomic displacements, octahedral tilts, and/or elastic distortions. Instead of a perfect long-range order, these structural features are correlated only over short length scales within nanoscale domains. The presence of such nanoscale domains and their relation to large functional properties has been reasonably explained for Pb-based ferroelectrics, although there still exist significant knowledge gaps [5,46]. Recent investigations are also bringing forth the potential central role that such nanoscale domains can play towards enhancing the electromechanical properties of new Pb-free ferroelectrics. One promising strategy could be the engineering of local structural disorder in such a way so as to induce large structural fluctuations under critical operating conditions. However, in order to successfully execute such an approach, it is a pre-requisite that the types of structural disorder in different Pb-free ferroelectrics, as well as how they respond to external stimuli such as electric fields or mechanical stress, are clearly understood. It needs to be mentioned here that due to differences in chemical bonding environments, the types of local structural disorders in the new Pb-free ferroelectrics are expected to be substantially different than those studied earlier for Pb-based ferroelectrics. For example, A-site displacements due to a more covalent Pb-O (A-O) bond drive ferroelectric distortion in Pb-based ferroelectrics. However, Ba-O and K-O bond has a more ionic character and therefore, <111> type Ti and Nb displacements are the dominant factors for ferroelectricity in BaTiO₃ and KNbO₃ [47,48]. It is thus warranted that external-stimuli-induced changes in nanoscale atomic ordering are investigated anew in Pb-free ferroelectrics.

The measurement and analyses of experimental signatures from nanoscale correlated disorders in materials are very different from those used in classical crystallography to determine long-range ordered structures [49]. Using tools of classical crystallography, the long-range atomic structure can be determined accurately by noting the position and the area of well-marked intense peaks in the diffraction pattern known as Bragg peaks. Instead, the correlated atomic disorder within nanoscale domains needs to be determined from the diffuse scattered intensities in between the Bragg peaks [49–51]. Diffraction experiments of high-quality single crystals enables measurement of such diffuse scattering signatures in reciprocal space in much more details than what can be achieved in polycrystalline powder samples. In this regard, a brief introduction to the origin of structured diffuse scattering for single-crystal diffraction is provided below.

In the presence of local disorders, the above Equation (1) can be modified as

$$I(\vec{Q}) = \sum_{n=1}^N \sum_{m=1}^N f_m f_n \exp\left(i\vec{Q} \cdot \left(\vec{R}_m + \vec{u}_m - \vec{R}_n - \vec{u}_n\right)\right) \quad (2)$$

where \vec{u}_m and \vec{u}_n refer to small displacements from the average positions of \vec{R}_m and \vec{R}_n [52,53]. Essentially, Equation (2) takes into account both chemical disorder on different atomic sites (f_m and f_n), as well as disorder in atomic displacements. If such disorder occurs in a truly random fashion, then it results in incoherent scattering, which contributes to the background. However, if there is short-range order present, either with regard to atomic site occupancies or atomic displacements, then well-defined diffuse scattering patterns are observed in addition to the Bragg peaks. Here, it can be seen that the diffuse scattering is also a function of \vec{Q} or the diffraction wave vector. Therefore, in order to better model the nanoscale ordered structures that give rise to patterned diffuse scattering within the different hkl reciprocal lattice planes, measurement of the same should be taken with clear distinction of \vec{Q} direction. This is only achievable with diffraction from single-crystal samples.

Below, I have reviewed some recent single-crystal diffraction studies in Pb-free ferroelectrics that have shed light on the kind of structural disorders present in these materials. In addition, examples of in situ experiments are provided that are enabling real-time investigation of how local structures evolve under external stimuli.

2.2.1. Atomic Displacement Disorder

Although not readily appreciated, atomic displacement disorder is broadly prevalent in solid solutions of Pb-free ferroelectrics such as BaTiO₃ and KNbO₃. These two prototypical compounds had been traditionally described as belonging to the displacive type ferroelectrics, in which the equilibrium positions of the B-site cation shifts off-center along a particular direction which matches with the average polarization for the respective phase, such as [001] in the tetragonal phase [2]. However, subsequent investigations overwhelmingly demonstrated that these exhibit characteristics partial to both displacive and order-disorder type ferroelectrics.

According to the order-disorder model, originally proposed by Comes et al., the B-site cation in BaTiO₃ and KNbO₃ is displaced in all phases along the $\langle 111 \rangle$ body diagonal directions, as illustrated in Figure 4 [54,55]. In the high-temperature cubic phase, displacements of B-site cation along all the $\langle 111 \rangle$ directions are equally probable, leading to no net polarization. With decreasing temperature, the degeneracy of the B-site cation displacements along the different body-diagonals is broken. In the ferroelectric tetragonal phase, B-site cation displacements are favored for only 4 of the 8 $\langle 111 \rangle$ directions, thereby leading to a net electrical polarization along [001] direction. At still lower temperatures in the ferroelectric orthorhombic phase, only 2 of the 8 $\langle 111 \rangle$ directions are favored, leading to a net polarization along [110]. In the ferroelectric rhombohedral ground-state phase at even lower temperatures, the structure is fully ordered with all B-site cation displacements along single [111] direction. The different correlations among the $\langle 111 \rangle$ B-atom displacements can be determined from the diffuse scattering patterns. 1-dimensional correlation of the $\langle 111 \rangle$ B-atom displacements along $\langle 100 \rangle$ crystallographic directions gives rise to sheets of diffuse scattering intensity in the {100} reciprocal lattice planes, such as shown in Figure 4c. Based on the types of atomic displacements in the different average crystallographic phase, one can therefore expect to have three sheets of diffuse scattering in the cubic phase, two such sheets in the tetragonal phase, and only one such sheet in the orthorhombic phase; since the atomic displacements are correlated over long-distances in the rhombohedral phase, no such diffuse scattering sheets are visible.

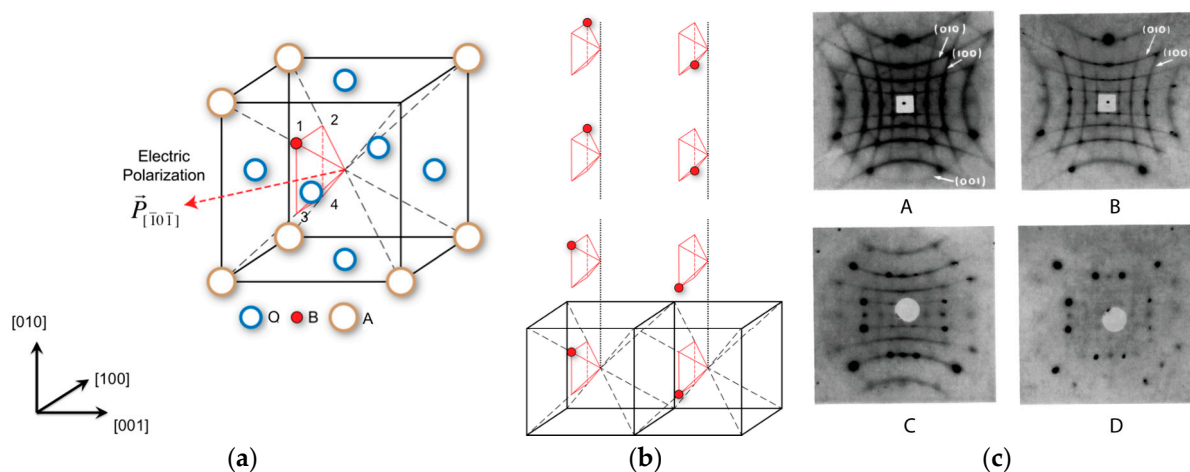


Figure 4. (a) The degenerate B atomic displacement in ABO₃ oxides is illustrated with particular reference to the orthorhombic phase of KNbO₃. The displacements along the possible $\langle 111 \rangle$ directions are marked by indices 1–4. (b) The B atomic displacements are correlated over short-range in the form of 1-dimensional chains. (c) The 1-dimensional chains give rise to {100} diffuse scattering sheets, which are observed as straight lines on an area detector. The scattering patterns measured with laboratory X-rays and an area detector are shown for cubic (A), tetragonal (B), orthorhombic (C), and rhombohedral (D) phases of a KNbO₃ crystal, after Comes et al. [54,55] Reproduced with permission from the International Union of Crystallography, <https://journals.iucr.org/>.

Based on the Scherrer equation, the thickness of the diffuse scattering sheets is inversely proportional to the correlation lengths of the atomic displacements ordering. The dimensions of the diffuse scattering sheets can be determined from 2-dimensional scattering patterns using an area detector, such as shown in Figure 5, thereby providing a semi-quantitative means to determine the length scales of atomic correlations in a material. Using single-crystal diffuse scattering measurements with laboratory X-rays, the 1-dimensional correlations among B-atom displacements in BaTiO₃ and KNbO₃ were earlier estimated to be between 50 Å and 100 Å [54,55]. More recent measurements with high-energy X-rays provide estimates of the order of 2 nm [56,57], which is closer to that predicted from theoretical calculations [58]. In addition to 1-dimensional correlations, 2-dimensional correlations in the form of nanoscale polar clusters among B-atom off-center displacements are also possible [59,60].

It is further proposed that the addition of different atomic substitutions can modify short-range correlations within these polar clusters with correlated B-site atomic displacements [61–63]. While there have been some microscopy studies on the modifying effects of solid solution additives on short-range correlations in BaTiO₃ and KNbO₃-based ferroelectric compositions, single-crystal diffuse scattering studies of these materials are however yet to be undertaken. There is therefore a lot of room to gain new knowledge about local atomic displacements ordering in these materials.

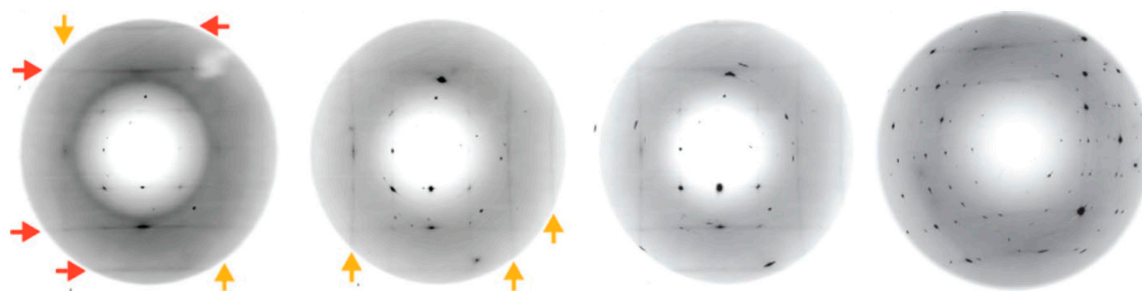


Figure 5. Single-crystal diffuse scattering pattern from a KNbO₃ single-crystal. The red and orange arrows indicate the diffuse scattering lines in the (010) and (100) reciprocal lattice plane, respectively. The {100} diffuse scattering lines became fainter with increasing pressure of 4.3 GPa, 6.3 GPa, 12.1 GPa (left-to-right), and finally disappeared at applied pressure of 21.8 GPa (extreme right). After Ravy et al. [56] Reprinted from reference [56] DOI: 10.1103/PhysRevB.99.117601, with permission from the American Physical Society.

Most remarkably, in situ diffraction with synchrotron X-rays have shown that the nanoscale correlations for atomic displacements in both BaTiO₃ and KNbO₃ are highly susceptible to applied pressure and electric fields. The susceptibility of B-site atomic displacements on applied pressure was studied by Ravy et al. from in situ high-energy X-ray diffraction experiments [56]. They showed that the intensity of the diffuse scattering lines, as described above, are strong functions of the magnitude of applied pressures. Such behavior can be described as a result of changes in both magnitude and correlations among B-site atomic displacements. Similarly, the effect of applied electric fields on B-site atomic displacement correlations in single-crystal KNbO₃ were shown by Pramanick et al. It was shown that application of a modest electric field of 300 V/mm in the room-temperature orthorhombic phase of KNbO₃ along [001] can drastically change the length scale of Nb displacements from ~2 nm to ~7 nm [57]. This was determined from changes in the thickness of diffuse scattering lines as a function of applied electric fields, such as Figure 6.

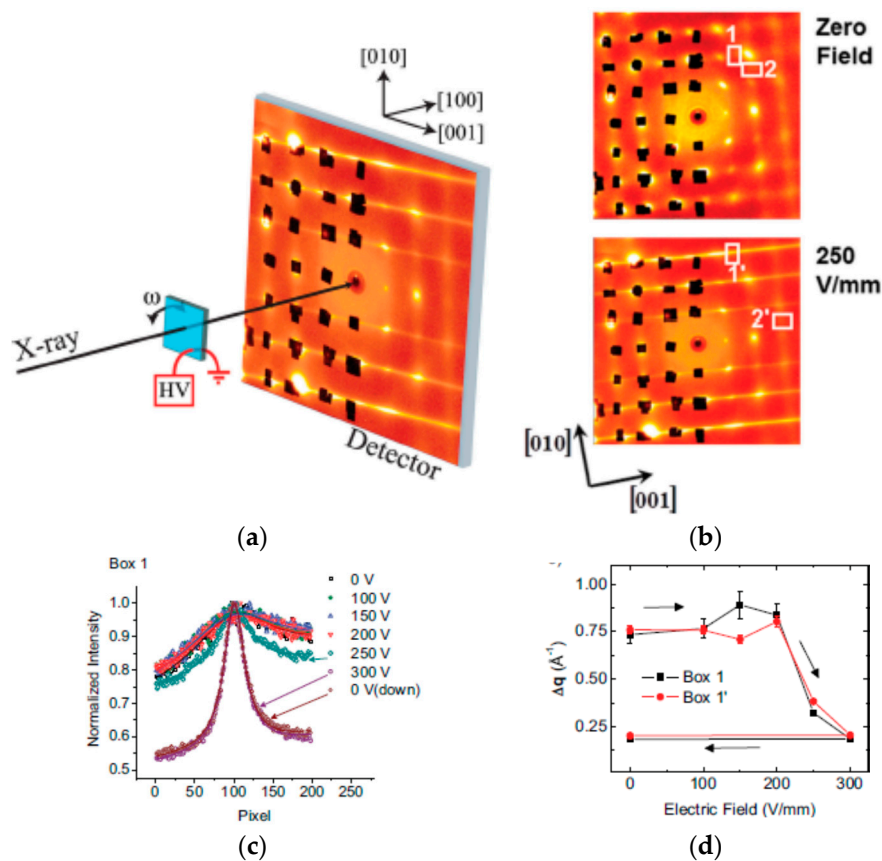


Figure 6. (a) Schematic illustration of an experimental set-up for an in situ measurement of single-crystal diffuse scattering pattern under applied electric fields using high-energy X-rays and a 2-dimensional area detector. In order to enhance the contrast for the diffuse scattering pattern, the Bragg diffraction spots are blocked with Pb tapes (shown in black). (b) Electric-field-induced change in diffuse scattering pattern. Quantitative characterization of length scale of atomic displacements correlations along different directions can be obtained based on integrated line profiles near different zone centers (ZC), marked by white boxes. (c) The integrated line profiles as function of applied electric fields, for box 1 near 022 ZC. (d) The full width at half maximum (FWHM) of the line profiles, plotted as Δq , is inversely proportional to the correlation length of the off-center B atom displacements. After Pramanick et al. [57] Reprinted from reference [57], with permission from John Wiley and Sons.

2.2.2. Octahedral Tilt Disorder

In addition to off-center atomic displacements, tilting of oxygen octahedra constitutes another defining feature for crystal structure of perovskite ferroelectrics. The various relations between octahedral tilting arrangements and average crystal symmetry were originally explained by Glazer [64]. The perovskite crystal lattice can be viewed as a network of corner linked BO_3 octahedra with interstitial A ions, such as illustrated in Figure 7a. The octahedra can be tilted (or rotated) around the crystallographic a , b , or c axes, which are identified as placeholders in the Glazer notation. If the unit cell dimensions along two axes are the same, then the same letter can be used for two space holders. The rotation of the adjacent octahedra along a tilting axis can be in phase (marked by superscript $+$) or antiphase (marked by superscript $-$). For no tilting, a superscript of 0 is used. For example, the octahedral tilting patterns for $a^0a^0c^+$ and $a^-b^-c^-$ are shown in Figure 7b and c, respectively.

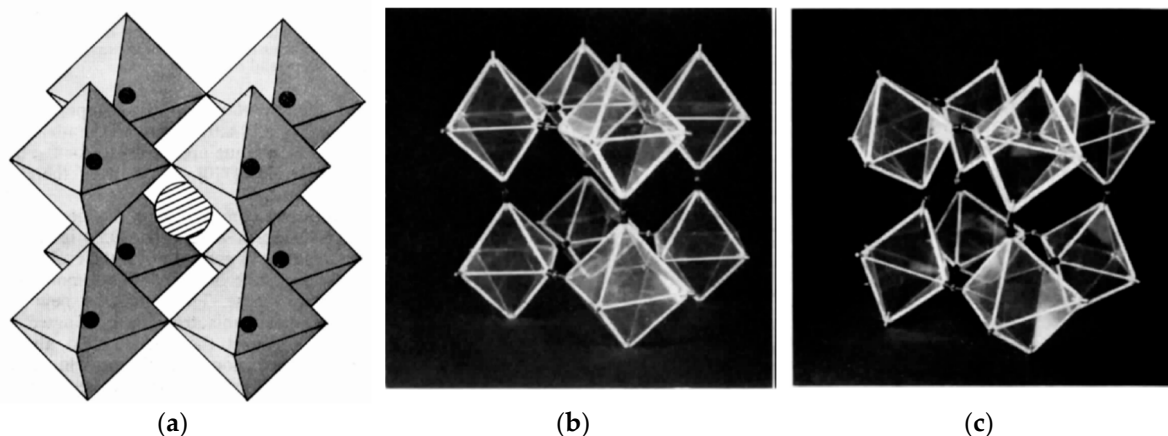


Figure 7. (a) The corner linked network of BO₃ octahedra with interstitial A ions. The B ions are shown in solid black circles, while the A ion is shown as striped circle. (b) Stereo-photograph of octahedral tilting pattern for $a^0a^0c^+$, where the adjacent octahedra along c axis are tilted in phase. (c) Stereo-photograph of octahedral tilting pattern for $a^-b^-c^-$, where the adjacent octahedra along all three axes are tilted in antiphase manner. After Glazer [64] Reprinted from reference [55] DOI: 10.1103/PhysRevB.99.117601, with permission from the American Physical Society.

The effect of oxygen octahedral tilting becomes particularly important for perovskite ferroelectrics with strong hybridization between s and p orbitals of the neighboring oxygen and A-site ions, such as in PZT. For Pb-free ferroelectrics, this is exemplified by the system Na_{0.5}Bi_{0.5}TiO₃ (NBT) and its solid solutions. The changes in the average crystal structure in this system comprise both re-orientation of the polarization direction, as well as the octahedral tilt arrangements [65,66]. Below the $T_C \sim 840$ K, Na_{0.5}Bi_{0.5}TiO₃ assumes a ferroelectric/ferrielectric phase with average polarization direction parallel to [001] and $a^0a^0c^+$ octahedral tilt arrangement. Upon cooling below $T \sim 570$ K, the system transitions to a ferroelectric phase with average rhombohedral symmetry, which is defined by polarization parallel to $\langle 111 \rangle$ and $a^-a^-a^-$ octahedral tilt arrangement. The lower temperature phase is also identified in some publications as having monoclinic symmetry, instead of rhombohedral, although that viewpoint is debated in other places [66–71]. In any case, it is now understood that Na_{0.5}Bi_{0.5}TiO₃ and its solid solutions exhibit considerable nanoscale disorder and therefore assertions of any long-range crystal symmetry for this system is going to be open to interpretations. Single-crystal X-ray and neutron diffraction of Na_{0.5}Bi_{0.5}TiO₃-based ferroelectrics has helped to clarify many of the subtleties in this system with regard to structural disorders.

The diffuse scattering pattern for the Na_{0.5}Bi_{0.5}TiO₃ system shows several interesting features such as described below [45,72–77]. Single-crystal diffraction revealed presence of diffuse scattering streaks, which are asymmetrically extended from the Bragg peaks along the lower-angular $\langle 001 \rangle$ directions. The peculiar extension of the streaks, as well as their intensities, are hkl -dependent. Based on detailed analyses of both X-ray and neutron diffuse scattering patterns from NBT single crystals, a general model could be proposed whereby the diffuse streaks are caused by the inclusion of nanoscale tetragonal plate-like structures within a rhombohedral matrix. Since the tetragonal and rhombohedral phases have different octahedral tilting arrangements, such an inclusion can be viewed as stacking faults separating adjacent rhombohedral regions. The reason for such tetragonal plate-like nanostructures is not entirely clear, although models based on atomic segregation similar to Guinier-Preston zones (GPZ) and memory effect leading to persistence of local regions of higher temperature phase have been proposed [45,76]. The asymmetric nature of the streaks has been tentatively explained as due to the slight expansion of the inclusions with respect to the matrix phase; nevertheless, the issue needs to be investigated further [76]. In addition to the asymmetric $\langle 001 \rangle$ diffuse scattering streaks, ridges of diffuse scattering were also observed with orientations along $\langle 110 \rangle$, which appear to be correlated with

the presence of random local fields similar to some Pb-based ferroelectrics [73]. Additionally, Huang scattering due to presence of long-range strain fields, supposedly caused by the presence of nanoscale inclusions, has also been noted [76]. All the diffuse scattering features were observed to be dependent on composition for $\text{Na}_{0.5}\text{Bi}_{0.5}\text{TiO}_3$ - BaTiO_3 (NBT-BT) solid solutions, which indicated a gradual transition from a shorter-to-longer range ordering of polar atomic displacements and octahedral tilting [77]. These observations indicate that ferroelectrics based on $\text{Na}_{0.5}\text{Bi}_{0.5}\text{TiO}_3$ are complex nanostructured oxides with hierarchical structures, which require extensive studies for their comprehensive understanding.

Most interestingly, similar to what is described in Section 2.2.1. A, the nanoscale structures showed strong susceptibility for changes under the application of external stimuli. Kreisel et al. showed from in situ high-energy X-ray diffraction experiments that application of hydrostatic pressure up to 2.8 GPa first leads to decrease in the intensity of the asymmetric diffuse scattering peaks in $\text{Na}_{0.5}\text{Bi}_{0.5}\text{TiO}_3$ single crystals, and finally to their eventual disappearance (Figure 8a) under 3.7 GPa [45]. Similar decrease in intensities of L-shaped asymmetric diffuse scattering peaks could also be observed in $\text{Na}_{0.5}\text{Bi}_{0.5}\text{TiO}_3$ single crystals under applied electric fields (Figure 8b) [78,79]. Such observations indicated that the structural differences between the matrix and the nanoscale inclusions could be irreversibly overcome by application of mechanical pressure or electric fields, ultimately leading to a phase transition in the short-range order associated with nanoscale inclusions.

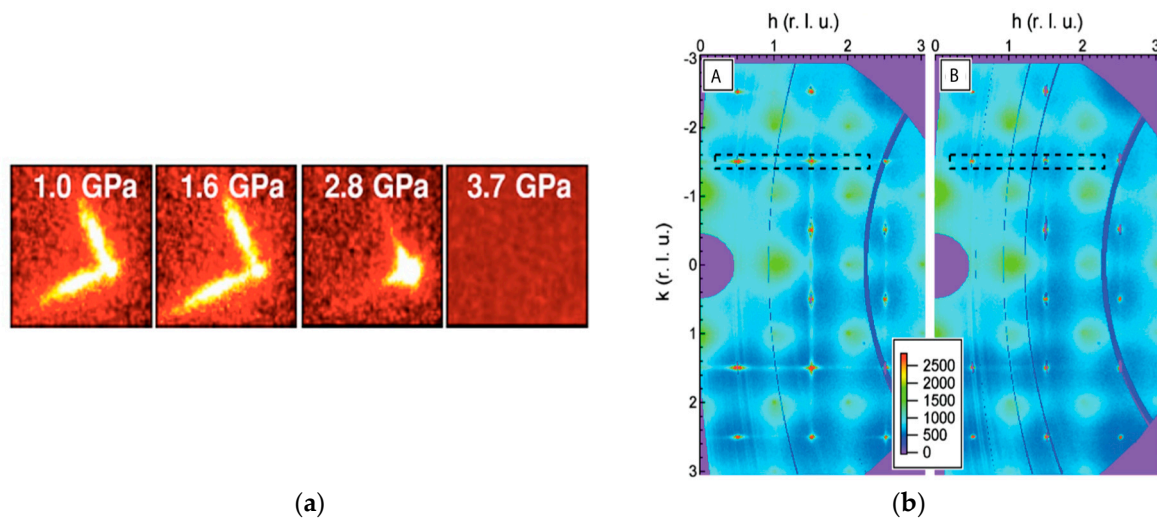


Figure 8. The diffuse scattering streaks in single-crystal diffraction pattern of $\text{Na}_{0.5}\text{Bi}_{0.5}\text{TiO}_3$ are proposed to come from nanoscale tetragonal inclusions within a rhombohedral matrix. (a) Weakening and eventual disappearance of diffuse streaks with increasing pressure. Reprinted from reference [45] DOI: 10.1103/PhysRevB.68.014113, with permission from the American Physical Society. (b) Similar effect observed for change in diffuse scattering patterns measured under zero field (A) and under electric field of 4.6 kV/mm (B). Reprinted from reference [78], with permission from AIP Publishing.

The above-mentioned changes in nanoscale structural correlations are significant since they have a direct effect on electromechanical susceptibility, as discussed in the following section. These initial studies on prototypical compounds have demonstrated that external field- or stress-induced changes in atomic displacements correlations should be studied in more detail in the solid solutions of these compounds. The availability of high quality single crystals will certainly be a facilitating factor for undertaking such studies.

2.3. Lattice Instability

The influence of nanoscale structural correlations towards macroscopic electromechanical properties of ferroelectrics can be better appreciated if fundamental relationships between the two are firmly

established in addition to the already apparent empirical relationships. However, establishing clear physical relationships between characteristics of nanoscale structural domains and electromechanical susceptibility is not straightforward and only a few examples of investigative studies exist in this area, such as reference [46]. The critical linkage between short-range atomic ordering within domains and macroscopic electromechanical susceptibility can be found through investigation of lattice vibration modes or phonons, which informs about the various inherent or evolving lattice instabilities. Inelastic neutron (and more recently, X-ray) scattering provides an excellent means for characterization of phonons in piezoelectric crystals. While strictly speaking this falls outside the scope of their current review, which is focused on diffraction or elastic scattering, a brief mention is made here of the characterization of phonons in Pb-free piezoelectric crystals in recognition of their perceived importance.

The central role of lattice dynamics towards the electromechanical properties of crystalline materials was originally recognized by Cochran [80]. From a basic viewpoint, it can be understood that the intrinsic susceptibility for mechanical deformation of a ferroelectric crystal is related to the elastic instability of the lattice [20], which is furthermore related to the propagation characteristics of long-wavelength acoustic phonon modes [81]. In gauging the effects of nanoscale ordered domains on electromechanical properties, one should therefore look at the correlations between structures and the propagation of acoustic phonon modes. Such investigations could indicate new pathways for designing new compositions of Pb-free ferroelectrics, as indicated from the following examples.

In prototypical KNbO_3 , it was demonstrated much earlier that the short-range correlations among the off-centered Nb displacements have a strong effect on the propagation of acoustic phonons; however, such effects could only be observed for phonons with shorter wavelengths or longer wavevectors ($q > 0.2$) [82]. In an interesting demonstration, using high-energy X-ray single-crystal diffraction and inelastic neutron scattering measurement, it was shown that when the correlation length for Nb-displacements is increased from ~ 2 nm to ~ 7 nm, the propagation of even longer wavelength (or shorter wavevector) acoustic phonons are damped in a transverse direction (see Figure 9) [57]. This indicated how controlling the dimensions of the nanoscale domains that are related to correlated atomic displacements could enhance the susceptibility for electromechanical shear deformation in this ferroelectric material. A similar effect of electric-field induced enhanced lattice instability was also demonstrated for BaTiO_3 single crystal [83].

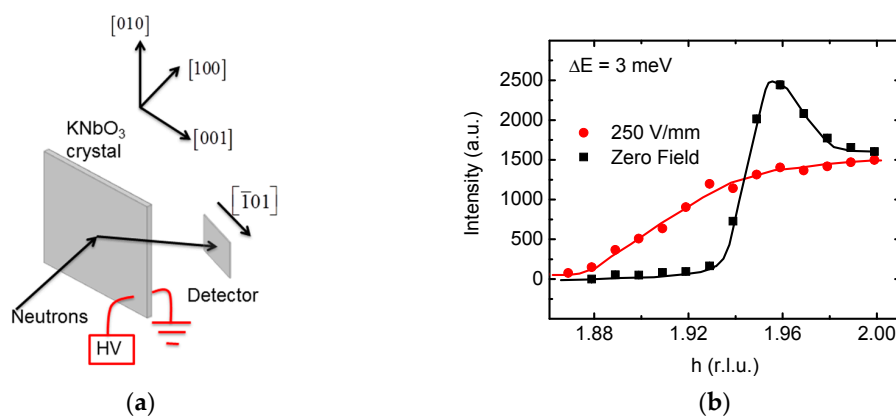


Figure 9. (a) Schematic illustration of in situ measurement of phonons in a crystal under applied electric fields. The geometry of the crystal is the same, as shown in Figure 6. The transverse acoustic modes propagating along $[101]$ direction were measured around the (202) ZC with a moving detector. This set up enables investigation of the effect of increased correlation length for B-atom displacements on transverse phonon propagation. (b) The dampening of the phonons, observed from a broadening of the inelastic neutron scattering peak, indicate increased lattice instability and hence greater susceptibility to mechanical deformation under field. After Pramanick et al. [57] Reprinted from reference [57], with permission from John Wiley and Sons.

In the case of $\text{Na}_{0.5}\text{Bi}_{0.5}\text{TiO}_3$, a recent inelastic neutron scattering study by Luo et al. indicated dynamic tilting modes of the oxygen octahedra, which are possibly coupled to the dimensions of the nanoscale domain structures [77]. Detailed in situ studies might show how short-range ordering of octahedral tilts and their dynamic vibrational modes evolve under applied electric fields or mechanical pressure, and therefore better elucidate the role of nanoscale domains on macroscopic electromechanical properties.

2.4. Domain Reorientation

In addition to the structural changes described above, re-orientation of microscopic domains can also significantly contribute to the macroscopic electromechanical response of a ferroelectric crystal [35,43]. It is therefore important to be able to characterize the nature and extent of domain reorientation in ferroelectric crystals under the application of an external stimulus. Single-crystal diffraction can provide clear and detailed insights into domain reorientation pathways, which are not readily obtainable from experiments on polycrystalline ceramics.

The basis for characterization of domain reorientation from single-crystal diffraction is explained below. In order to maintain continuity across a domain boundary, the two adjacent ferroelectric domains in a ferroelectric crystal are misoriented by a certain angular range, which is defined by crystallographic considerations. For example, in tetragonal crystals, the misorientation angle is $\theta \sim 2 \tan^{-1}(c/a)$ between the ferroelectric domains separated by non-180° domain walls [84], where c and a are the crystallographic unit cell parameters, as schematically illustrated in Figure 10. This effect causes splitting of the diffraction peaks coming from the different domain variants in the crystal. Based on the relative intensities of the symmetry-related diffraction spots, the volume fraction for the different domain variants can be estimated. This is illustrated below for the case of domain switching phenomena in $\text{Na}_{0.5}\text{Bi}_{0.5}\text{TiO}_3$ single crystals.

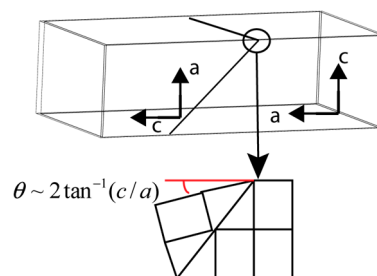


Figure 10. Schematic illustration of the misorientation angle between two domains separated by a non-180° domain wall in a tetragonal crystal.

Using high-energy synchrotron X-rays, Kitanaka et al. studied the microscopic mechanism for polarization switching in $\text{Na}_{0.5}\text{Bi}_{0.5}\text{TiO}_3$ single crystals under electric fields applied parallel to $\langle 100 \rangle$ and $\langle 111 \rangle$ directions [85]. Based on the differences in intensities of the symmetry-related diffraction spots, such as shown in Figure 11, it was demonstrated that polarization switching in both cases was dominated by step-wise non-180° (71° and/or 109°) domain switching processes. A preference for 71° reorientation of the polarization direction was furthermore asserted based on theoretical calculations using DFT.

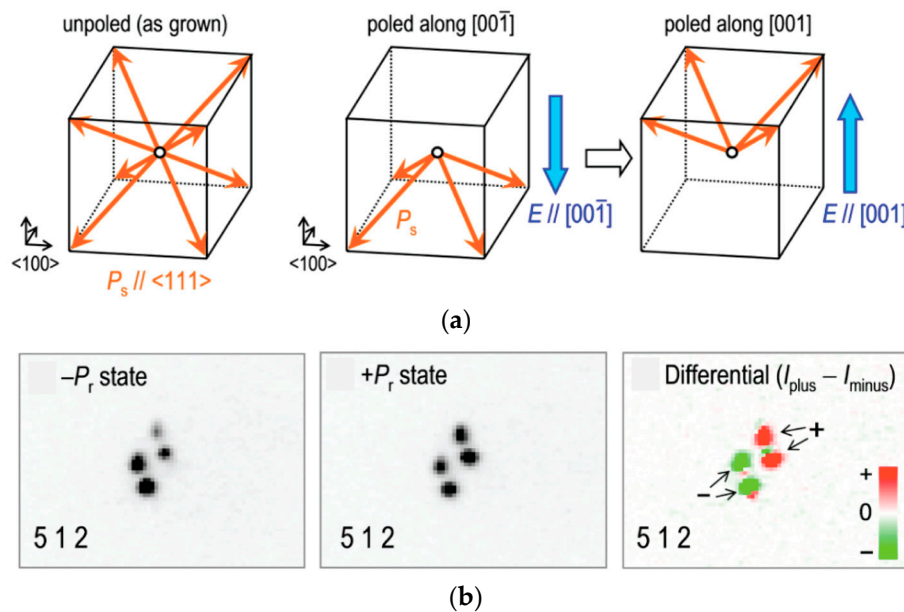


Figure 11. (a) The eight equivalent directions for polarization vector P_s in rhombohedral $\text{Na}_{0.5}\text{Bi}_{0.5}\text{TiO}_3$ and their preferred states under applied electric fields. (b) Changes in scattering intensities of the symmetry related diffraction spots coming from domain variants with polarization directions as indicated in the top panel. A non-equivalence of the diffraction spots for electric fields applied parallel to $[00\bar{1}]$ and $[001]$ indicates non- 180° domain reorientation processes for polarization switching. After Kitanaka et al. [84]. Reprinted from reference [85] DOI: 10.1103/PhysRevB.89.104104, with permission from the American Physical Society.

A similar investigation of polarization switching behavior in $\text{K}_{0.25}\text{Na}_{0.75}\text{NbO}_3$ single-crystals was undertaken by Deng et al. [86]. The macroscopic symmetry for this crystal was determined to be of monoclinic C type, with the spontaneous polarization direction close to $\langle 054 \rangle$. Based on both single-crystal X-ray diffraction and polarized light microscopy, it was determined that polarization switching is again dominated by non- 180° domain reorientations processes. This was evident from change in relative intensities of the symmetry-related diffraction intensities of $(101)_{\text{pc}}$ reflections from a (101) oriented crystal for different amplitudes of applied electric fields.

3. Opportunities and Challenges

Above, I have reviewed some recent developments with regard to the characterization of Pb-free piezoelectric materials using single-crystal X-ray and neutron diffraction. These studies have broadened our understanding of structure-property relationships in this new class of materials and further opened up new avenues of investigation. In fact, they have shown that the science of correlating complex materials chemistry with local bonding environments, multiscale structural disorders, and ultimately, electromechanical properties under applied stimuli for the new Pb-free piezoelectric materials is still in its infancy. In this regard, there exists huge opportunities to gain new knowledge in this area. As reviewed above, single-crystal diffraction can be a very effective characterization technique for this purpose, especially under in situ experimental conditions.

It needs to be mentioned here that care must be taken while analyzing single-crystal diffraction data for characterization of multi-scale structural changes. If measurements are specifically focused near single ZC, it might lead to incorrect conclusions. For example, additional spots can appear near a ZC due to either change in symmetry due to a crystallographic phase transition (or distortion) or non- 180° domain reorientation. A comprehensive survey of a broad region of reciprocal space is therefore necessary. This is facilitated by two significant developments in terms of instrumental capabilities. With the advent of 3rd generation synchrotron and high-energy X-rays, large areas of

reciprocal space can be surveyed in minutes. This is due to the fact that for small X-ray wavelengths (~ 0.1 Å), the Ewald sphere is essentially flat, and therefore reflections within a single hkl plane can be obtained in a single shot [52]. Secondly, neutron Laue diffraction is gaining in popularity with the advent of spallation sources and time-of-flight Laue diffractometers. Modern instruments, such as TOPAZ at the Spallation Neutron Source (SNS), have extensive area-detector coverage that are capable of three-dimensional \vec{Q} -space mapping from a stationary single crystal [87]. In a time-of-flight neutron diffractometer, the scattering intensities from the crystal appear at the detector at different times of flight, which correspond to different wavelengths, and therefore to different wave vectors \vec{Q} . Consequently, in addition to resolving the scattered intensities in two dimensions with the use of area detectors, scattering intensities are also recorded by the arrival times of the neutrons at the detector. In this manner, the three-dimensional scattering patterns can be obtained very effectively without the need for any rotation of the crystal during data collection. These advancements in instrumental capabilities also open the possibility to conduct time-resolved experiments, which will enable characterization of transient states during application of external stimuli. In addition, care must be taken to distinguish between elastic diffuse scattering, which informs about the static local disorder in a material and the inelastic scattering which informs about the dynamic structural states. This is often not possible for X-ray instruments, where the scattering intensities are integrated over all possible energy-transfers. Modern neutron scattering instruments at spallation sources, such as CORELLI at SNS [88], affords the possibility for such a distinction between elastic and inelastic diffuse scattering. Finally, one must also be careful to account for intensity changes due to changes in internal strains and extinction effects, while analyzing diffraction data from single-crystal samples.

It goes without saying that the availability of good-quality single-crystals is a must for undertaking comprehensive structural measurements. This means that the sample should be of adequate dimension for a specific experimental purpose. Measurement of inelastic signals and diffuse scattering often needs larger samples as compared to measurement of Bragg diffraction peaks. Additionally, the samples should be properly annealed to reduce internal stress related effects. At the very least, the sample preparation procedures must be clearly explained. Additionally, if the experimental goal is to obtain diffraction data for precise structural refinement, then it is better that the single-crystal sample contains a single domain or twin variant. However, this requirement could be relaxed by comprehensive data collection over large area of the reciprocal space and properly indexing the peaks from different domain variants using advanced software [87].

With continuing improvements in the areas of single-crystal growth techniques and capabilities of scattering instruments, it should be possible to significantly advance our understanding of the fundamental physico-chemical principles that drive large enhancements in Pb-free piezoelectrics, and therefore, to accelerate their discovery process.

Acknowledgments: A.P. gratefully acknowledges funding support from CityU (Project Numbers 7200514, 7004967 and 9610377).

Conflicts of Interest: The authors declare no conflict of interest.

References

1. Newnham, R.E. *Properties of Materials*; Newnham, Oxford University Press: Oxford, UK, 2005.
2. Lines, M.E.; Glass, A.M. *Principles and Applications of Ferroelectrics and Related Materials*; Clarendon Press: Oxford, UK, 2002.
3. Setter, N. *Piezoelectric Materials in Devices*; Ceramics Laboratory, EPFL: Lausanne, Switzerland, 2002.
4. Uchino, K. *Ferroelectric Devices*; Marcel Dekker: New York, NY, USA, 2000.
5. Zhang, S.; Li, F. High performance ferroelectric relaxor-PbTiO₃ single crystals: Status and perspective. *J. Appl. Phys.* **2012**, *111*, 031301. [[CrossRef](#)]
6. Rodel, J.; Jo, W.; Seifert, K.T.P.; Anton, E.-M.; Granzow, T. Perspective on the development of lead-free piezoceramic. *J. Am. Ceram. Soc.* **2009**, *92*, 1153–1177. [[CrossRef](#)]

7. EU-Directive 2002/95/EC: Restriction of the Use of Certain Hazardous Substances in Electrical and Electronic Equipment (RoHS); Off J Eur Union 2003; European Union: Brussels, Belgium, 2003; Volume 46, pp. 19–37. Available online: <http://data.europa.eu/eli/dir/2002/95/oj>.
8. EU-Directive 2011/65/EC: Restriction of the Use of Certain Hazardous Substances in Electrical and Electronic Equipment (RoHS); Off J Eur Union 2011; European Union: Brussels, Belgium, 2011; Volume 54, pp. 88–110. Available online: <http://data.europa.eu/eli/dir/2011/65/oj>.
9. Directive (EU) 2017/2102 of the European Parliament and of the Council of 15 November 2017 Amending Directive 2011/65/EU on the Restriction of the Use of Certain Hazardous Substances in Electrical and Electronic Equipment; Off J Eur Union 2017; European Union: Brussels, Belgium, 2017; Volume 60, pp. 8–11. Available online: <http://data.europa.eu/eli/dir/2017/2102/oj>.
10. Measures for the Administration on Pollution Control of Electronic Information Products, Ministry of Information Industry China Order No. 39, 2006. Available online: http://www.fdi.gov.cn/1800000121_39_4733_0_7.html.
11. Rodel, J.; Webber, K.G.; Dittmer, R.; Jo, W.; Kimura, M.; Damjanovic, D. Transferring lead-free piezoelectric ceramics into applications. *J. Eur. Ceram. Soc.* **2015**, *35*, 1659–1681. [[CrossRef](#)]
12. Saito, Y.; Takao, H.; Tani, T.; Nonoyama, T.; Takatori, K.; Homma, T.; Nagaya, T.; Nakamura, M. Lead-free piezoceramics. *Nature* **2004**, *432*, 84–87. [[CrossRef](#)] [[PubMed](#)]
13. Zhang, S.T.; Koumga, A.B.; Aulbach, E.; Ehrenberg, H.; Rodel, J. Giant strain in lead-free piezoceramics Bi_{0.5}Na_{0.5}TiO₃-BaTiO₃-K_{0.5}Na_{0.5}NbO₃ system. *Appl. Phys. Lett.* **2007**, *91*, 112906. [[CrossRef](#)]
14. Liu, W.F.; Ren, X.B. Large piezoelectric effect in Pb-free ceramics. *Phys. Rev. Lett.* **2009**, *103*, 257602. [[CrossRef](#)] [[PubMed](#)]
15. Rao, W.-F.; Wang, Y.U. Domain wall broadening mechanism for domain size effect of enhanced piezoelectricity in crystallographically engineered ferroelectric single crystals. *Appl. Phys. Lett.* **2007**, *90*, 041915. [[CrossRef](#)]
16. Bhattacharya, S.; Jinschek, J.R.; Cao, H.; Wang, Y.U.; Li, J.; Viehland, D. Direct high-resolution transmission electron microscopy observation of tetragonal nanotwins within the monoclinic M_C phase of Pb(Mg_{1/3}Nb_{2/3})O₃-0.35PbTiO₃ crystals. *Appl. Phys. Lett.* **2008**, *92*, 142904. [[CrossRef](#)]
17. Sluka, T.; Tagantsev, A.K.; Damjanovic, D.; Gureev, M.; Setter, N. Enhanced electromechanical response of ferroelectrics due to charged domain walls. *Nat. Commun.* **2012**, *3*, 748. [[CrossRef](#)] [[PubMed](#)]
18. Gu, Y.; Xue, F.; Lei, S.; Lummen, T.T.A.; Wang, J.; Gopalan, V.; Chen, L.-Q. Monoclinic phases arising across thermal inter-ferroelectric phase transitions. *Phys. Rev. B* **2014**, *90*, 024104. [[CrossRef](#)]
19. Shao, Y.-T.; Zuo, J.-M. Lattice-Rotation vortex at the charged monoclinic domain boundary in a relaxor ferroelectric crystal. *Phys. Rev. Lett.* **2017**, *118*, 15. [[CrossRef](#)] [[PubMed](#)]
20. Davis, M.; Budimir, M.; Damjanovic, D.; Setter, N. Rotator and extender ferroelectrics: Importance of the shear coefficient to the piezoelectric properties of domain-engineered crystals and ceramics. *J. Appl. Phys.* **2007**, *101*, 054112. [[CrossRef](#)]
21. Wada, S.; Yako, K.; Kakemoto, H.; Tsurumi, T.; Kiguchi, T. Enhanced piezoelectric properties of barium titanate single crystals with different engineered-domain sizes. *J. Appl. Phys.* **2005**, *98*, 014109. [[CrossRef](#)]
22. Wada, S.; Kakemoto, H.; Tsurumi, T. Enhanced piezoelectric properties of piezoelectric single crystals by domain engineering. *Mater. Trans.* **2004**, *45*, 178–187. [[CrossRef](#)]
23. Li, X.; Chen, C.; Deng, H.; Zhang, H.; Lin, D.; Zhao, X.; Luo, H. The growth and properties of lead-free ferroelectric single crystals. *Crystals* **2015**, *5*, 172–192. [[CrossRef](#)]
24. Chen, K.; Xu, G.; Yang, D.; Wang, X.; Li, J. Dielectric and piezoelectric properties of lead-free 0.95(K_{0.5}Na_{0.5})NbO₃-0.05LiNbO₃ crystals grown by Bridgman method. *J. Appl. Phys.* **2007**, *101*, 044103. [[CrossRef](#)]
25. Fu, D.; Itoh, M.; Koshihara, S.-Y. Crystal growth and piezoelectricity of BaTiO₃-CaTiO₃ solid solution. *Appl. Phys. Lett.* **2008**, *93*, 012904. [[CrossRef](#)]
26. Zeng, Y.; Zheng, Y.; Tu, X.; Lu, Z.; Shi, E. Growth and characterization of lead-free Ba_(1-x)Ca_xTi_(1-y)Zr_yO₃ single crystal. *J. Cryst. Growth* **2012**, *343*, 17–20. [[CrossRef](#)]
27. Singh, G.; Bhaumick, I.; Ganesamoorthy, S.; Bhatt, R.; Karnal, A.K.; Tiwari, V.S.; Gupta, P.K. Electro-caloric effect in 0.45BaZr_{0.2}Ti_{0.8}O₃-0.55Ba_{0.7}Ca_{0.3}TiO₃ single crystal. *Appl. Phys. Lett.* **2013**, *102*, 082902. [[CrossRef](#)]
28. Fisher, J.G.; Bencan, A.; Holc, J.; Kosec, M.; Vernay, S.; Rytz, D. Growth of potassium sodium niobate single crystals by solid state crystal growth. *J. Cryst. Growth* **2007**, *303*, 487–492. [[CrossRef](#)]
29. Zheng, L.; Huo, X.; Wang, R.; Wang, J.; Jiang, W.; Cao, W. Large size and lead-free (Na,K)(Nb,Ta)O₃ piezoelectric single crystal: Growth and full tensor properties. *CrystEngComm* **2013**, *15*, 7718. [[CrossRef](#)]

30. Ogino, M.; Noguchi, Y.; Kitanaka, Y.; Miyayama, M.; Moriyoshi, C.; Kuroiwa, Y. Polarization rotation and monoclinic distortion in ferroelectric $(\text{Bi}_{0.5}\text{Na}_{0.5})\text{TiO}_3\text{-BaTiO}_3$ single crystals under electric field. *Crystals* **2014**, *4*, 273–295. [[CrossRef](#)]
31. Jiang, M.; Randall, C.A.; Guo, H.; Rao, G.; Tu, R.; Gu, Z.; Cheng, G.; Liu, X.; Zhang, J.; Li, Y. Seed-free solid-state growth of large lead-free piezoelectric single crystals: $(\text{Na}_{1/2}\text{K}_{1/2})\text{NbO}_3$. *J. Am. Ceram. Soc.* **2015**, *98*, 2988–2996. [[CrossRef](#)]
32. Yang, J.; Zhang, F.; Yang, Q.; Liu, Z.; Li, Y.; Liu, Y.; Zhang, Q. Large piezoelectric properties in KNN-based lead-free single crystals grown by a seed-free solid-state crystal growth method. *Appl. Phys. Lett.* **2016**, *108*, 182904. [[CrossRef](#)]
33. Ahn, C.-W.; Lee, H.-Y.; Han, G.; Zhang, S.; Choi, S.-Y.; Choi, J.J.; Kim, J.-W.; Yoon, W.-H.; Choi, J.-H.; Park, D.-S.; et al. Self-growth of centimeter scale single crystals by normal sintering process in modified potassium sodium niobate ceramics. *Sci. Rep.* **2015**, *5*, 17656. [[CrossRef](#)] [[PubMed](#)]
34. Kang, S.-J.L.; Park, J.-H.; Ko, S.-Y.; Lee, H.-Y. Solid-state conversion of single-crystals: The principle and the state-of-the-art. *J. Am. Ceram. Soc.* **2015**, *98*, 347–360. [[CrossRef](#)]
35. Damjanovic, D. Contributions to the piezoelectric effect in ferroelectric single crystals and ceramics. *J. Am. Ceram. Soc.* **2005**, *88*, 2663. [[CrossRef](#)]
36. Pramanick, A.; Damjanovic, D.; Daniels, J.E.; Nino, J.C.; Jones, J.L. Origins of electro-mechanical coupling in polycrystalline ferroelectrics during subcoercive electrical loading. *J. Am. Ceram. Soc.* **2011**, *94*, 293–309. [[CrossRef](#)]
37. Jones, J.L. The use of diffraction in the characterization of piezoelectric materials. *J. Electroceram.* **2007**, *19*, 69–81. [[CrossRef](#)]
38. Noheda, B.; Cox, D.E.; Shirane, G.; Park, S.-E.; Cross, L.E.; Zhong, Z. Polarization rotation via a monoclinic phase in the piezoelectric $92\%\text{PbZn}_{1/3}\text{Nb}_{2/3}\text{O}_3\text{-}8\%\text{PbTiO}_3$. *Phys. Rev. Lett.* **2001**, *86*, 3891. [[CrossRef](#)] [[PubMed](#)]
39. Daniels, J.E.; Finlayson, T.R.; Davis, M.; Damjanovic, D.; Studer, A.J.; Hoffman, M.; Jones, J.L. Neutron diffraction study of the polarization reversal mechanism in $[111]_c$ -oriented $\text{Pb}(\text{Zn}_{1/3}\text{Nb}_{2/3})\text{O}_3\text{-}x\text{PbTiO}_3$. *J. Appl. Phys.* **2007**, *101*, 104108. [[CrossRef](#)]
40. Pramanick, A.; Stoica, A.D.; An, K. High-resolution 2-D Bragg diffraction reveal heterogeneous domain transformation behavior in a bulk relaxor ferroelectric. *Appl. Phys. Lett.* **2016**, *109*, 092907. [[CrossRef](#)]
41. Esteves, G.; Fancher, C.M.; Jones, J.L. In situ characterization of polycrystalline ferroelectrics using X-ray and neutron diffraction. *J. Mater. Res.* **2015**, *30*, 340. [[CrossRef](#)]
42. Fuentes-Cobas, L.E.; Montero-Cabrera, M.E.; Pardo, L.; Fuentes-Montero, L. Ferroelectrics under the synchrotron light: A review. *Materials* **2016**, *9*, 14. [[CrossRef](#)] [[PubMed](#)]
43. Cullity, B.D. *Elements of X-ray Diffraction*; Prentice Hall: Upper Saddle River, NJ, USA, 2001.
44. Pramanick, A.; Jones, J.L.; Tutuncu, G.; Ghosh, D.; Stoica, A.D.; An, K. Strain incompatibility and residual strains in ferroelectric single crystals. *Sci. Rep.* **2012**, *2*, 929. [[CrossRef](#)] [[PubMed](#)]
45. Kreisel, J.; Bouvier, P.; Dkhil, B.; Thomas, P.A.; Glazer, A.M.; Welberry, T.R.; Chaabane, B.; Mezouar, M. High-pressure X-ray scattering of oxides with a nanoscale local structure: Application to $\text{Na}_{1/2}\text{Bi}_{1/2}\text{TiO}_3$. *Phys. Rev. B* **2003**, *68*, 014113. [[CrossRef](#)]
46. Xu, G.; Wen, J.; Stock, C.; Gehring, P.M. Phase instability induced by polar nanoregions in a relaxor ferroelectric system. *Nat. Mater.* **2008**, *7*, 562–566. [[CrossRef](#)] [[PubMed](#)]
47. Cohen, R.E. Origin of ferroelectricity in perovskite oxides. *Nature* **1992**, *358*, 136–138. [[CrossRef](#)]
48. Cohen, R.E.; Krakauer, H. Lattice dynamics and origin of ferroelectricity in BaTiO_3 : Linearized-augmented-plane-wave total-energy calculations. *Phys. Rev. B* **1990**, *42*, 6416–6423. [[CrossRef](#)]
49. Keen, D.A.; Goodwin, A.L. The crystallography of correlated disorder. *Nature* **2015**, *521*, 303–309. [[CrossRef](#)] [[PubMed](#)]
50. Egami, T.; Billinge, S.J.L. *Underneath the Bragg Peaks*, 2nd ed.; Pergamon: Oxford, UK, 2012.
51. Welberry, T.R.; Goossens, D.J. Diffuse scattering and partial disorder in complex structures. *IUCr* **2014**, *1*, 550. [[CrossRef](#)] [[PubMed](#)]
52. Ramsteiner, I.B.; Schops, A.; Reichert, H.; Dosch, H.; Honkimaki, V.; Zhong, Z.; Hastings, J.B. High-energy X-ray diffuse scattering. *J. Appl. Cryst.* **2009**, *A42*, 392–400. [[CrossRef](#)]
53. Welberry, T.R. *Diffuse X-ray Scattering and Models of Disorder*; Oxford University Press: Oxford, UK, 2004.

54. Comes, R.; Lambert, M.; Guinier, A. The chain structure of BaTiO₃ and KNbO₃. *Sol. State Commun.* **1968**, *6*, 715–719. [[CrossRef](#)]
55. Comes, R.; Lambert, M.; Guinier, A. Désordre linéaire des cristaux (cas du Silicium, du Quartz, et des Pérovskites Ferroélectriques). *Acta Crystallogr. A* **1970**, *26*, 244–254. [[CrossRef](#)]
56. Ravy, S.; Itié, J.-P.; Polian, A.; Hanfland, H. High-pressure study of X-ray diffuse scattering in ferroelectric perovskites. *Phys. Rev. Lett.* **2007**, *99*, 117601. [[CrossRef](#)] [[PubMed](#)]
57. Pramanick, A.; Jørgensen, M.R.V.; Diallo, S.O.; Christianson, A.D.; Fernandez-Baca, J.A.; Hoffmann, C.; Wang, X.; Lan, S.; Wang, X.-L. Nanoscale atomic displacements ordering for enhanced piezoelectric properties in lead-free ABO₃ ferroelectrics. *Adv. Mater.* **2015**, *27*, 4330–4335. [[CrossRef](#)] [[PubMed](#)]
58. Yu, R.; Krakauer, H. First-principles determination of chain-structure instability in KNbO₃. *Phys. Rev. Lett.* **1995**, *74*, 4067. [[CrossRef](#)] [[PubMed](#)]
59. Tsuda, K.; Yasuhara, A.; Tanaka, M. Two-dimensional mapping of polarizations of rhombohedral nanostructures in the tetragonal phase of BaTiO₃ by the combined use of the scanning transmission electron microscopy and convergent-beam electron diffraction methods. *Appl. Phys. Lett.* **2013**, *103*, 082908. [[CrossRef](#)]
60. Pramanick, A.; Wang, X.P.; Hoffmann, C.; Diallo, S.O.; Jørgensen, M.R.V.; Wang, X.-L. Microdomain dynamics in single-crystal BaTiO₃ during paraelectric-ferroelectric phase transition measured with time-of-flight neutron scattering. *Phys. Rev. B* **2015**, *92*, 174103. [[CrossRef](#)]
61. Simon, A.; Ravez, J.; Maglione, M. The crossover from a ferroelectric to a relaxor state in lead-free solid solutions. *J. Phys. Condens. Matter* **2004**, *16*, 963–970. [[CrossRef](#)]
62. Liu, Y.; Withers, R.L.; Nguyen, B.; Elliot, K. Structurally frustrated polar nanoregions in BaTiO₃-based relaxor ferroelectric systems. *Appl. Phys. Lett.* **2007**, *91*, 152907. [[CrossRef](#)]
63. Akbarzadeh, A.R.; Prosandeev, S.; Walter, E.J.; Al-Barakaty, A.; Bellaiche, L. Finite-temperature properties of Ba(Zr,Ti)O₃ relaxors from first principles. *Phys. Rev. Lett.* **2012**, *108*, 257601. [[CrossRef](#)] [[PubMed](#)]
64. Glazer, A.M. Simple ways of determining perovskite structures. *Acta Cryst. A* **1975**, *31*, 756–762. [[CrossRef](#)]
65. Jones, G.O.; Thomas, P.A. The tetragonal phase of Na_{0.5}Bi_{0.5}TiO₃—A new variant of the perovskite structure. *Acta Cryst. B* **2000**, *56*, 426–430. [[CrossRef](#)]
66. Jones, G.O.; Thomas, P.A. Investigation of the structure and phase transitions in the novel A-site substituted distorted perovskite compound Na_{0.5}Bi_{0.5}TiO₃. *Acta Cryst. B* **2002**, *58*, 168–178. [[CrossRef](#)]
67. Aksel, E.; Forrester, J.S.; Jones, J.L.; Thomas, P.A.; Page, K.; Suchomel, M.R. Monoclinic crystal structure of polycrystalline Na_{0.5}Bi_{0.5}TiO₃. *Appl. Phys. Lett.* **2011**, *98*, 152901. [[CrossRef](#)]
68. Aksel, E.; Forrester, J.S.; Kowalski, B.; Jones, J.L.; Thomas, P.A. Phase transition sequence in sodium bismuth titanate observed using high-resolution X-ray diffraction. *Appl. Phys. Lett.* **2011**, *99*, 222901. [[CrossRef](#)]
69. Ma, C.; Guo, H.; Tan, X. A new phase boundary in (Bi_{1/2}Na_{1/2})TiO₃-BaTiO₃ revealed via a novel method of electron diffraction analysis. *Adv. Funct. Mater.* **2013**, *23*, 5261–5266. [[CrossRef](#)]
70. Maurya, D.; Murayama, M.; Pramanick, A.; Reynolds, W.T., Jr.; An, K.; Priya, S. Origin of high piezoelectric response in A-site disordered morphotropic phase boundary composition of lead-free piezoelectric 0.93(Na_{0.5}Bi_{0.5})TiO₃-0.07BaTiO₃. *J. Appl. Phys.* **2013**, *113*, 114101. [[CrossRef](#)]
71. Beanland, R.; Thomas, P.A. Symmetry and defects in single-crystalline Na_{0.5}Bi_{0.5}TiO₃. *Phys. Rev. B* **2014**, *89*, 174102. [[CrossRef](#)]
72. Thomas, P.A.; Trujillo, S.; Boudard, M.; Gorfman, S.; Kreisel, J. Diffuse X-ray scattering in the lead-free piezoelectric crystals Na_{1/2}Bi_{1/2}TiO₃ and Ba-doped Na_{1/2}Bi_{1/2}TiO₃. *Solid State Sci.* **2010**, *12*, 311–317. [[CrossRef](#)]
73. Ge, W.; Devreugd, C.P.; Phelan, D.; Zhang, Q.; Ahart, M.; Li, J.; Luo, H.; Boatner, L.A.; Viehland, D.; Gehring, P.M. Lead-free and lead-based ABO₃ perovskite relaxors with mixed-valence A-site and B-site disorder: Comparative neutron scattering structural study of (N_{1/2}Bi_{1/2})TiO₃ and Pb(Mg_{1/3}Nb_{2/3})O₃. *Phys. Rev. B* **2013**, *88*, 174115. [[CrossRef](#)]
74. Chen, C.-S.; Chen, P.-Y.; Tu, C.-S. Polar nanoregions and dielectric properties in high-strain lead-free 0.93(Bi_{1/2}Na_{1/2})TiO₃-0.07BaTiO₃ piezoelectric single crystals. *J. Appl. Phys.* **2014**, *115*, 014105. [[CrossRef](#)]
75. Zhang, H.; Deng, G.; Studer, A.J.; Li, X.; Zhao, X.; Luo, H. Neutron diffuse scattering of (1-x)(Na_{0.5}Bi_{0.5})TiO₃-xBaTiO₃ relaxor ferroelectric single crystals. *Scr. Mater.* **2014**, *86*, 5–8. [[CrossRef](#)]
76. Gorfman, S.; Keeble, D.S.; Bombardi, A.; Thomas, P.A. Topology and temperature dependence of the diffuse X-ray scattering in Na_{0.5}Bi_{0.5}TiO₃ ferroelectric single crystals. *J. Appl. Cryst.* **2015**, *48*, 1543–1550.

77. Luo, C.; Bansal, D.; Li, J.; Viehland, D.; Winn, B.; Ren, Y.; Li, X.; Luo, H.; Delaire, O. Neutron and X-ray scattering study of phonon dispersion and diffuse scattering in $(\text{Na,Ba})\text{TiO}_3-x\text{BaTiO}_3$ single crystals near the morphotropic phase boundary. *Phys. Rev. B* **2017**, *96*, 174108. [[CrossRef](#)]
78. Daniels, J.E.; Jo, W.; Rodel, J.; Rytz, D.; Donner, W. Structural origins of relaxor behavior in a $0.96(\text{Bi}_{1/2}\text{Na}_{1/2})\text{TiO}_3-0.04\text{BaTiO}_3$ single crystal under electric field. *Appl. Phys. Lett.* **2011**, *98*, 252904. [[CrossRef](#)]
79. Daniels, J.E.; Jo, W.; Donner, W. High-energy synchrotron X-ray diffraction for in situ diffuse scattering studies of bulk single crystals. *JOM* **2012**, *64*, 174–180. [[CrossRef](#)]
80. Cochran, W. Crystal stability and the theory of ferroelectricity. *Adv. Phys.* **1960**, *9*, 387–423. [[CrossRef](#)]
81. Kittel, C. *Introduction to Solid State Physics*; John Wiley & Sons, Inc.: Hoboken, NJ, USA, 2005.
82. Currat, R.; Comes, R.; Dorner, B.; Wiesendanger, E. Inelastic neutron scattering in orthorhombic KNbO_3 . *J. Phys. C Solid State Phys.* **1974**, *7*, 2521. [[CrossRef](#)]
83. Pramanick, A.; Diallo, S.O.; Delaire, O.; Calder, S.; Christianson, A.D.; Wang, X.-L.; Fernandez-Baca, J.A. Origins of large enhancement in electromechanical coupling for nonpolar directions in ferroelectric BaTiO_3 . *Phys. Rev. B* **2013**, *88*, 180101(R). [[CrossRef](#)]
84. Pramanick, A.; Prewitt, A.D.; Forrester, J.S.; Jones, J.L. Domains, domain walls and defects in perovskite ferroelectric oxides: A review of present understanding and recent contributions. *Crit. Rev. Solid State Mater. Sci.* **2012**, *37*, 243–275. [[CrossRef](#)]
85. Kitanaka, Y.; Yanai, K.; Noguchi, Y.; Miyayama, M.; Kagawa, Y.; Moriyoshi, C.; Kuroiwa, Y. Non- 180° polarization rotation of ferroelectric $(\text{Bi}_{0.5}\text{Na}_{0.5})\text{TiO}_3$ single crystals under electric field. *Phys. Rev. B* **2014**, *89*, 104104. [[CrossRef](#)]
86. Deng, H.; Zhang, H.; Zhao, X.; Chen, C.; Wang, X.; Li, X.; Lin, D.; Ren, B.; Jiao, J.; Luo, H. Direct observation of monoclinic ferroelectric phase and domain switching process in $(\text{K}_{0.25}\text{Na}_{0.75})\text{NbO}_3$ single crystals. *CrstEngComm* **2015**, *17*, 2872–2877. [[CrossRef](#)]
87. Pramanick, A.; Wang, X.; An, K.; Stoica, A.; Yi, J.; Gai, Z.; Hoffmann, C.; Wang, X.-L. Structural modulations and magnetic properties of off-stoichiometric Ni-Mn-Ga magnetic shape memory alloys. *Phys. Rev. B* **2012**, *85*, 144412. [[CrossRef](#)]
88. Rosenkranz, S.; Osborn, R. Corelli: Efficient single crystal diffraction with elastic discrimination. *PRAMANA J. Phys.* **2008**, *71*, 705–711. [[CrossRef](#)]



© 2018 by the author. Licensee MDPI, Basel, Switzerland. This article is an open access article distributed under the terms and conditions of the Creative Commons Attribution (CC BY) license (<http://creativecommons.org/licenses/by/4.0/>).